JACS
JOURNAL OF THE AMERICAN CHEMICAL SOCIETY

Article

Multicolor Activatable Raman Probes for Simultaneous Detection of Plural Enzyme Activities

Hiroyoshi Fujioka, Jingwen Shou, Ryosuke Kojima, Yasuteru Urano, Yasuyuki Ozeki,* and Mako Kamiya*

Cite This: https://dx.doi.org/10.1021/jacs.0c09200

Read Online

ACCESS | 📊 Metrics & More | 📰 Article Recommendations | ⓢ Supporting Information

ABSTRACT: Raman probes based on alkyne or nitrile tags hold promise for highly multiplexed imaging. However, sensing of enzyme activities with Raman probes is difficult because few mechanisms are available to modulate the vibrational response. Here we present a general strategy to prepare activatable Raman probes that show enhanced Raman signals due to electronic preresonance (EPR) upon reaction with enzymes under physiological conditions. We identified a xanthene derivative bearing a nitrile group at position 9 (9CN-JCP) as a suitable scaffold dye, and synthesized four types of activatable Raman probes, which are targeted to different enzymes (three aminopeptidases and a glycosidase) and tuned to different vibrational frequencies by isotope editing of the nitrile group. We validated the activation of the Raman signals of these probes by the target enzymes and succeeded in simultaneous imaging of the four enzyme activities in live cells. Different cell lines showed different patterns of these enzyme activities.
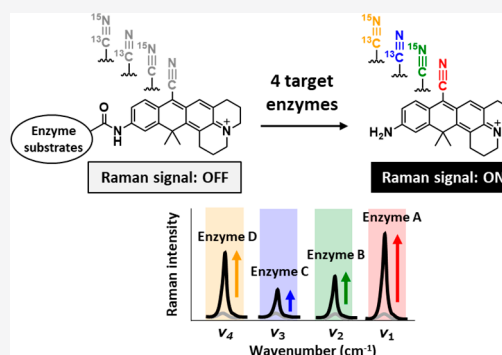
■ INTRODUCTION

Raman microscopy, which can characterize molecular species by detecting the vibrations of chemical bonds, has been developed as an important imaging modality to characterize cellular biochemical constituents without labeling.[1−3] Although the imaging speed of Raman microscopy has been limited by the weak signal intensity of spontaneous Raman scattering, the emergence and evolution of stimulated Raman scattering (SRS) microscopy, which exploits two-color laser pulses (the pump beam and the Stokes beam), has improved the sensitivity by several orders of magnitude, enabling high-speed Raman imaging.[4−6] Moreover, in the past decade, various Raman tags, including alkyne, nitrile and the carbon−deuterium bond, which show characteristic vibrational frequencies in the cell-silent region (1800−2800 cm^{-1}), have been developed for bioorthogonal imaging of small-molecular metabolites in live cells and tissues.[7−9]

Further, compared to fluorescence imaging, which suffers from a "color barrier" (i.e., the number of simultaneously resolvable targets is limited to four to six) owing to the intrinsically broad fluorescence peaks, Raman imaging has superior potential for highly multiplexed detection[10] because the Raman spectral line width can be 50−200 times smaller than the fluorescence peak width. Min et al. have achieved supermultiplexed vibrational imaging with two kinds of Raman probes, called MARS[11] and Carbow.[12] In addition, SRS imaging with MARS dyes can utilize the electronic preresonance (EPR) effect[13] to enhance the Raman signal by

∼10^3 times, by positioning the pump wavelength at 100−200 nm longer wavelength than the molecular absorption maximum. The EPR-SRS strategy provides submicromolar sensitivity, together with spatial resolution comparable to that of typical confocal fluorescence microscopy, and thus is suitable for observing low-abundance molecules in cells.

However, most pre-existing Raman probes show constant Raman signal intensity ("always-on" Raman probes), and thus their application has been limited to labeling tags. Although there are a few reports of Raman probes that show a shift in Raman frequency (in response to a change of pH,[14] or the presence of hydrogen sulfide[15]) or that show Raman signal activation by chemically producing alkynes in a lipid bilayer via external addition of reagents,[16] it has generally been believed that the Raman signal cannot be switched on or off, because it arises from molecular vibration. Therefore, "activatable-type" Raman probes that can react with endogenous biological targets and show an increased Raman signal under physiological conditions have not been developed.

Here we set out to establish a first-in-class general design strategy of multicolor activatable Raman probes for simulta-
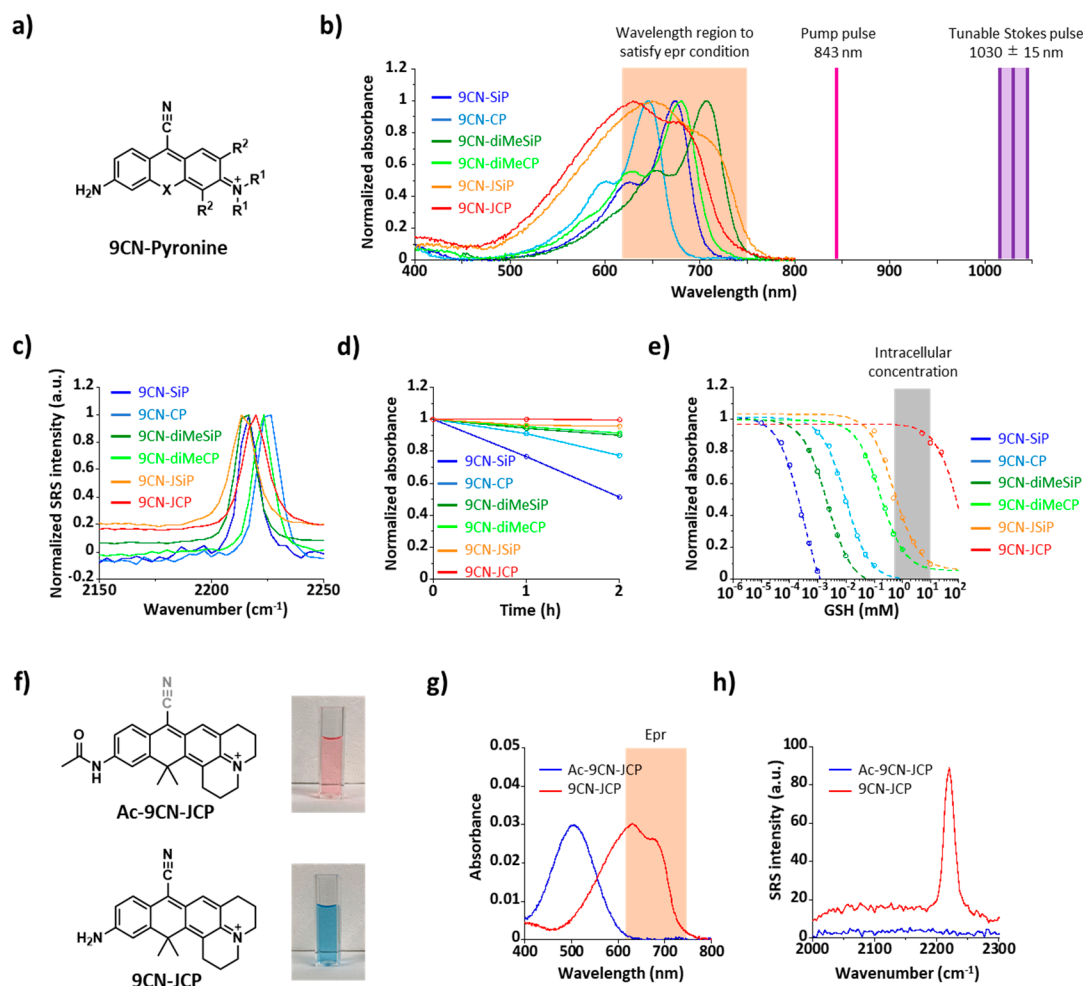
Figure 1. 9CN-pyronines as scaffold dyes of activatable Raman probes. (a) Chemical structures of 9CN-pyronines (see Table 1 for detailed chemical structures and compound names). (b) Normalized absorption spectra of 9CN-pyronines measured in PBS (pH 7.4) containing 0.1% DMSO as a cosolvent. (c) Normalized SRS spectra of 1 mM 9CN-pyronines measured in DMSO. (d) Time-dependent changes in the absorbance of 9CN-pyronines measured in 200 mM sodium phosphate buffer (pH 7.4) containing 0.1% DMSO as a cosolvent. (e) Dose−response curves of 9CN-pyronines versus GSH concentration (0−25 mM). Absorbance was normalized at the wavelength of the respective absorption maxima shown in Table 1. (f) Chemical structures of Ac-9CN-JCP and 9CN-JCP. The pictures showed 10 μM solutions of Ac-9CN-JCP and 9CN-JCP in PBS (pH 7.4). (g) Absorption spectra of 1 μM Ac-9CN-JCP and 9CN-JCP measured in PBS (pH 7.4) containing 0.1% DMSO as a cosolvent. (h) SRS spectra of 1 mM Ac-9CN-JCP and 9CN-JCP measured in PBS (pH 7.4) containing 10% DMSO as a cosolvent.

neous detection of plural biomolecules. For this purpose, we focused on the phenomenon that the Raman signal intensity is remarkably enhanced under EPR conditions compared to that under electronic nonresonance conditions. Considering that the wavelength of the pump beam in a typical SRS system is around 800−900 nm, we speculated that the Raman signal intensity could be "switched on", i.e., highly activated, when the molecular absorption of dyes exhibiting a Raman signal is shifted from the visible (electronic nonresonance condition) to the near-infrared (NIR) region (EPR condition) upon reaction with the target biomolecules. To develop activatable Raman probes based on this molecular design, we focused on the activities of hydrolases in living cells, because it is well-known that specific enzyme-catalyzed hydrolysis reactions can induce significant absorption shifts of colorimetric/fluorogenic substrates.[17] We synthesized a series of Raman-active xanthene derivatives, and among them we identified a suitable scaffold for developing activatable Raman probes to target enzyme activities. On the basis of this scaffold, we then prepared four activatable Raman probes with distinct Raman peaks, which
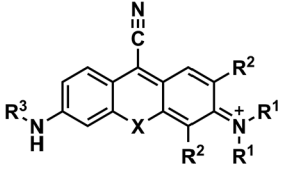
exhibit Raman signal activation upon reaction with selected enzymes of interest both in vitro and in living cells, and succeeded in the simultaneous detection of plural enzyme activities.

RESULTS AND DISCUSSION

Design of a Scaffold Dye for EPR-SRS Imaging in Live Cells. To develop activatable Raman imaging probes that show a red shift in absorption from the visible (electronic nonresonance condition) to the NIR region (EPR condition) upon reaction with enzymes, we first searched for a suitable scaffold dye. For this purpose, we focused on xanthene derivatives with the nitrile at the 9th position (9CN-pyronines), because they display a single, sharp, and strong Raman peak in the cell-silent region (1800−2800 cm^{-1}) under EPR conditions.[11] To switch the Raman signal intensity on and off, we prepared a series of symmetric and asymmetric 9CN-pyronines bearing a primary aromatic amine at the C3 position that would be available for conjugating enzyme substrate moieties via an amide bond to blue-shift the molecular

absorption[18] (Figure 1a, Table 1, Schemes S1–S6). Considering that the wavelength of the pump beam in our SRS

Table 1. Photochemical Properties of 9CN-Pyronines

compound	X	R^1	R^2	R^3	λ_{abs} [nm][a]	ω_R [cm^{-1}][b]
9CN-SiP	SiMe$_2$	H	H	H	673	2217
9CN-CP	CMe$_2$	H	H	H	646	2227
9CN-diMeSiP	SiMe$_2$	Me	H	H	708	2216
9CN-diMeCP	CMe$_2$	Me	H	H	680	2223
9CN-JSiP	SiMe$_2$	–(CH$_2$)$_3$–	H		650	2214
9CN-JCP	CMe$_2$	–(CH$_2$)$_3$–	H		630	2220
Ac-9CN-JCP	CMe$_2$	–(CH$_2$)$_3$–	CH$_3$CO		506	n.d.[c]

[a]Measured in PBS (pH 7.4) containing 0.1% DMSO as a cosolvent. [b]Measured in DMSO. [c]n.d. means not detected under 1 mM condition. λ_{abs}: Absorption maximum. ω_R: Raman wavenumber of C≡N vibrational mode.

imaging system is fixed at 843 nm to acquire Raman signals in the 2000–2300 cm^{-1} region (Figure S1),[19] the wavelength region of molecular absorption appropriate for EPR is expected to be 620–750 nm (see Supporting Information).[11] As it has been reported that 9CN-xanthenes with oxygen (O) at the 10th position tend to exhibit relatively short wavelengths,[20,21] we focused on silicon (Si) or carbon (C) as the atom at the 10th position of xanthene (X in Figure 1a). For *N*-substitution at C6, we selected a primary amine (for 9CN-SiP, 9CN-CP), an *N,N*-dimethylamine (for 9CN-diMeSiP, 9CN-diMeCP), or a julolidine-like structure (for 9CN-JSiP, 9CN-JCP). All of the synthesized compounds exhibited suitable absorption spectra that overlapped well with the EPR region and showed sufficiently strong SRS signals in the silent region under EPR conditions (Figure 1b,c, Table 1). Among these derivatives, 9CN-JSiP and 9CN-JCP, which have julolidine-like structure, exhibited distinct spectra in terms of both peak positions and band widths; this may be due to the environmental sensitivity of these derivatives, because they showed red-shifted absorption spectra in DMSO (Figure S2). Next, we examined the stability of these 9CN-pyronines under physiological conditions by evaluating their stability in phosphate buffer at pH 7.4 and their resistance to glutathione (GSH), one of the major antioxidants in cells. Because some pyronines are attacked at the 9th carbon atom of the xanthene ring by intracellular nucleophiles such as H$_2$O or GSH,[22] and these reactions convert the dyes to a colorless form, we thought this would lead to an electronic nonresonance state with a reduced Raman response. When we examined the stability in phosphate buffer at pH 7.4, the absorbance of 9CN-SiP and 9CN-CP significantly decreased after 2 h incubation at room temperature, with formation of the respective xanthones, due to the nucleophilic attack of H$_2$O (Figure 1d, Figure S3). As regards resistance to GSH, the intracellular GSH concentration is reported to be in the sub-millimolar to a few millimolar range,[23] so we expected that scaffold dyes which show constant NIR absorbance even in the presence of millimolar concentrations of GSH would be favorable for stable

measurement. We examined the dependence of the absorbance of these 9CN-pyronines on GSH concentration (Figure 1e). Most of the 9CN-pyronines showed a significant decrease of absorbance in the presence of millimolar concentrations of GSH. Among them, only 9CN-JCP exhibited sufficiently high absorbance, suggesting that it would be stable under physiological conditions. Thus, we selected 9CN-JCP as a candidate scaffold dye and prepared its acetylated derivative, Ac-9CN-JCP, as a model enzyme substrate (Figure 1f, Scheme S7).

Next, we compared the absorption spectra of Ac-9CN-JCP and 9CN-JCP in phosphate-buffered saline at pH 7.4 (PBS) (Figure 1g). As expected, Ac-9CN-JCP exhibited a blue-shifted absorption spectrum (absorption maximum at 506 nm in PBS); thus, a hypsochromic shift of more than 100 nm was induced by the acetylation of 9CN-JCP. The blue-shifted absorption of Ac-9CN-JCP is within the electronic non-resonance region, while that of 9CN-JCP is within the EPR region. In principle, such a molecular absorption shift should induce a large change of Raman signals. To confirm that this is the case, we next measured the SRS spectra of 1 mM Ac-9CN-JCP and 1 mM 9CN-JCP in PBS. Indeed, a remarkable change of SRS signal intensity was observed; Ac-9CN-JCP showed no peak, while 9CN-JCP showed a clear single peak (Figure 1h). Moreover, the RIE (relative Raman intensity vs EdU)[24] value of 9CN-JCP under EPR conditions was calculated to be about 87, which is much higher than those of alkynes and diynes under nonresonance conditions, whereas Ac-9CN-JCP under nonresonance conditions was calculated to be about 1.5 (Figure S4). These results support the idea that the Raman signal can be activated by controlling the electronic resonance via molecular absorption shift and indicate that 9CN-JCP is a promising scaffold for developing activatable Raman probes to observe enzyme activities.

Development of Multicolor Activatable Raman Probes for Plural Enzyme Activities. On the basis of the newly developed 9CN-JCP scaffold, we next isotopically edited the atoms of nitrile group on 9CN-JCPs to prepare 9C^{15}N-JCP, 9^{13}CN-JCP, and 9^{13}C^{15}N-JCP, to shift the vibrational resonances[8] (Figure 2a, Scheme S8). As expected, these isotope-edited 9CN-JCPs exhibited single sharp Raman peaks at distinct wavenumbers (Figure 2b). We further examined whether these SRS signals can be identified as four separate peaks even when the compounds are mixed. As expected, the SRS spectrum of the solution mixture showed four separate peaks, even though the absorption and fluorescence spectra of the compounds were identical (Figure 2c, Figure S5). Encouraged by these promising results, we next prepared four activatable Raman probes targeted to different enzymes by replacing the acetyl group of Ac-9CN-JCP with appropriate enzyme substrate moieties. We incorporated a γ-L-glutamyl (gGlu), L-leucyl (Leu), L-glutamyl-L-prolyl (EP), or β-D-galactosyl (βGal) group into the isotope-edited 9CN-JCPs via an amide bond or a carbamate linker to target γ-glutamyl transpeptidase (GGT), leucine aminopeptidase (LAP), dipeptidyl peptidase-4 (DPP-4), and β-galactosidase (β-Gal), respectively (Figure 2a, Schemes S9–S12). We confirmed that these probes (gGlu-9CN-JCP, Leu-9C^{15}N-JCP, EP-9^{13}CN-JCP, βGal-9^{13}C^{15}N-JCP) exhibited relatively short-wavelength absorption similar to that of Ac-9CN-JCP but were converted to the respective scaffolds (9CN-JCP, 9C^{15}N-JCP, 9^{13}CN-JCP, 9^{13}C^{15}N-JCP) upon reaction with corresponding target enzymes, resulting in a significant red shift in absorption
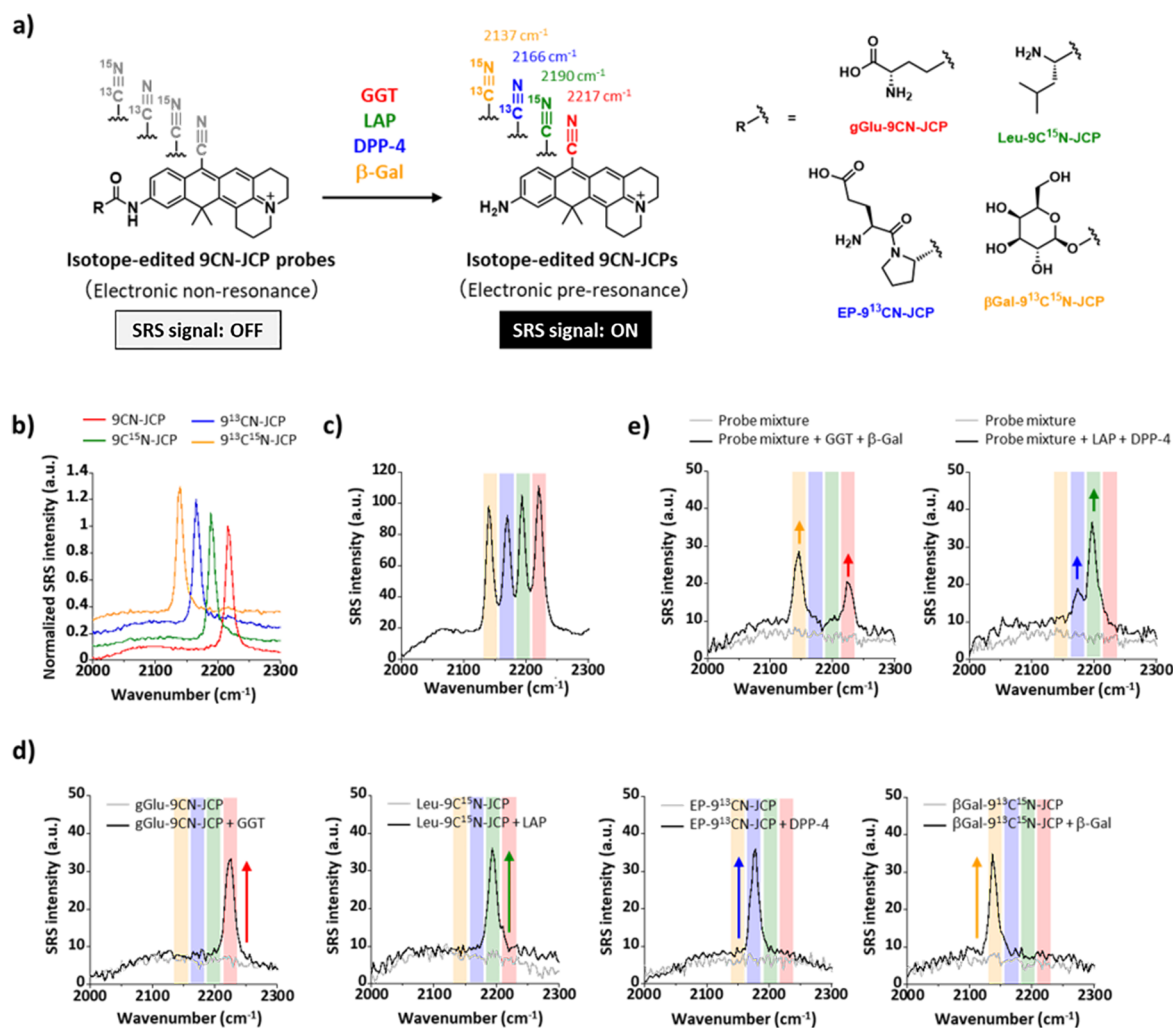
Figure 2. Development of activatable Raman probes for enzyme activities based on isotope-edited 9CN-JCPs. (a) Molecular design of activatable Raman probes based on isotope-edited 9CN-JCPs (9CN-JCP (red), 9C^{15}N-JCP (green), 9^{13}CN-JCP (blue), 9^{13}C^{15}N-JCP (yellow)). Raman signals from 9CN-JCP-based probes are activated upon reaction of the probe with the target enzyme because the absorption is shifted from the visible (electronic nonresonance conditions) to the NIR region (EPR conditions). gGlu-9CN-JCP for γ-glutamyl transpeptidase (GGT), Leu-9C^{15}N-JCP for leucine aminopeptidase (LAP), EP-9^{13}CN-JCP for dipeptidyl peptidase-4 (DPP-4), βGal-9^{13}C^{15}N-JCP for β-galactosidase (β-Gal). (b) Normalized SRS spectra of 1 mM isotope-edited 9CN-JCPs measured in DMSO. The spectra are vertically offset for clarity. (c) SRS spectrum of a mixture of the isotope-edited 9CN-JCPs (250 μM each) measured in DMSO. Highlights represent the regions of vibrational frequency of 9CN-JCP (red), 9C^{15}N-JCP (green), 9^{13}CN-JCP (blue), and 9^{13}C^{15}N-JCP (yellow). (d) SRS spectra of 1 mM gGlu-9CN-JCP, Leu-9C^{15}N-JCP, EP-9^{13}CN-JCP or βGal-9^{13}C^{15}N-JCP before (gray) and after (black) reaction with 1 unit of GGT, 0.12 units of LAP, 0.022 units of DPP-4, or 1 unit of β-Gal measured in PBS (pH 7.4) containing 10% DMSO as a cosolvent. Reaction solutions were incubated for 1 h at room temperature. (e) SRS spectra of a mixture of the isotope-edited 9CN-JCP probes (250 μM each) before (gray) and after (black) reaction with 5 units of GGT and 10 units of β-Gal (left) or with 0.12 units of LAP and 0.044 units of DPP-4 (right) measured in PBS (pH 7.4) containing 10% DMSO as a cosolvent. Reaction solutions were incubated for 1 h at room temperature.

(Figures S6–S9). We also confirmed that the Raman signal of each probe was significantly activated upon enzyme reaction, and the vibrational frequencies (2217 cm^{-1}, 2190 cm^{-1}, 2166 cm^{-1}, 2137 cm^{-1}) corresponded to the vibrational frequencies of the triple bond of 9CN-JCP, 9C^{15}N-JCP, 9^{13}CN-JCP, and 9^{13}C^{15}N-JCP in PBS (Figure 2d). We also confirmed that the activation of these probes was inhibited by coincubation with inhibitors of the corresponding enzymes (Figures S6–S9), and the Raman signal intensity produced by gGlu-9CN-JCP was linearly correlated with the concentration of GGT, demonstrating the suitability of this system for quantitative detection (Figure S10). To our knowledge, this is the first demonstration of activatable Raman probes that can report the activities of various hydrolases under physiological conditions.

We next examined whether the four different enzyme activities can be evaluated simultaneously by using a mixture of 9CN-JCP probes (gGlu-9CN-JCP, Leu-9C^{15}N-JCP, EP-9^{13}CN-JCP, βGal-9^{13}C^{15}N-JCP). Indeed, we observed specific SRS signal activation by the corresponding enzyme activities. Specifically, SRS signals of 9CN-JCP (2217 cm^{-1}) and 9^{13}C^{15}N-JCP (2137 cm^{-1}) were detected in the presence of GGT and β-Gal, and SRS signals of 9C^{15}N-JCP (2190 cm^{-1}) and 9^{13}CN-JCP (2166 cm^{-1}) were detected in the presence of LAP and DPP-4 (Figure 2e). These results indicate that isotope-edited 9CN-JCP-based activatable Raman probes can simultaneously detect plural enzyme activities.

Multicolor Imaging of Target Enzyme Activities in Live Cells. Next, we examined the applicability of our isotope-
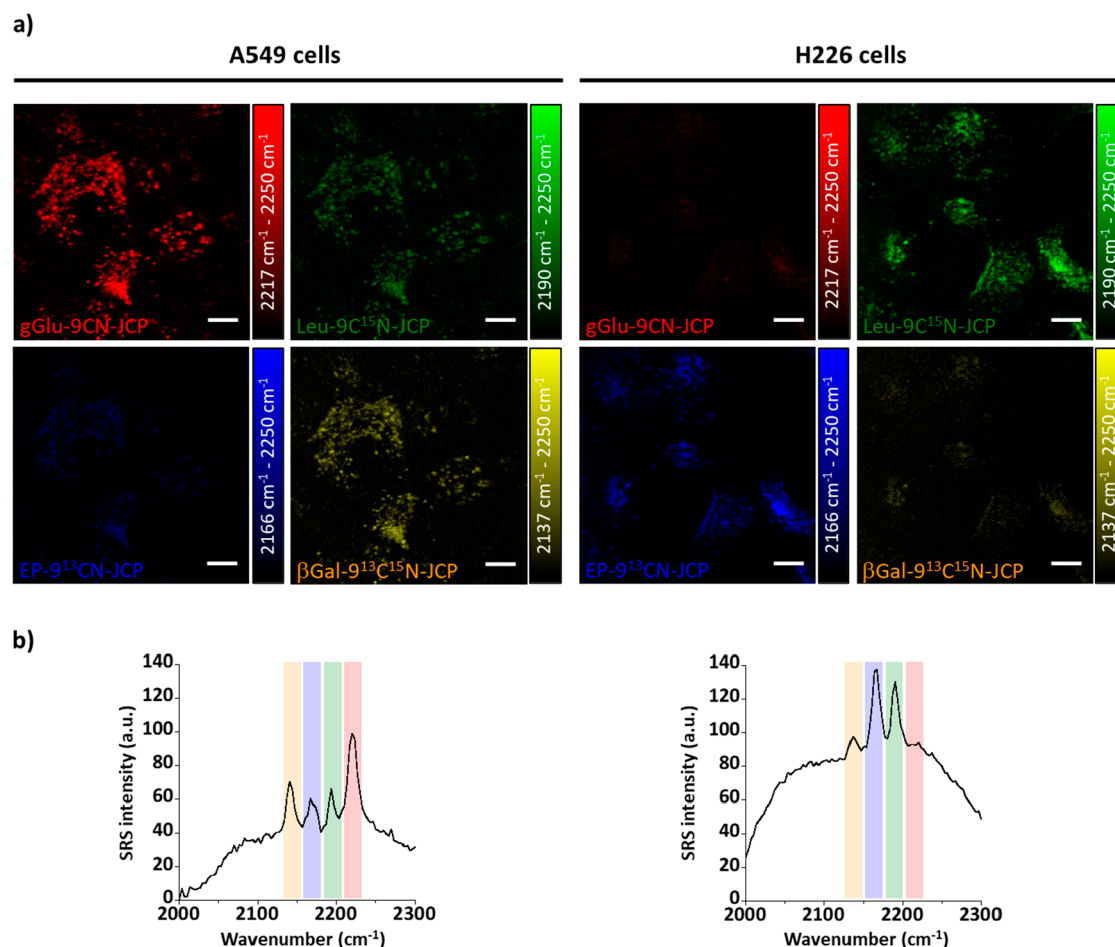
Figure 3. Simultaneous detection of the four enzyme activities in live cells by SRS imaging. A549 cells (left) and H226 cells (right) cells were incubated with 10 μM gGlu-9CN-JCP, Leu-9C^{15}N-JCP, and EP-9^{13}CN-JCP, and 20 μM βGal-9^{13}C^{15}N-JCP in HBSS (+) containing 0.5% DMSO as a cosolvent for 30 min. (a) SRS images of the four enzyme activities in A549 cells (left) and H226 cells (right). Images were obtained at 2217 cm^{-1} for gGlu-9CN-JCP, 2190 cm^{-1} for Leu-9C^{15}N-JCP, 2166 cm^{-1} for EP-9^{13}CN-JCP, and 2137 cm^{-1} for βGal-9^{13}C^{15}N-JCP. The background image at 2250 cm^{-1} was subtracted in each case. Scale bar: 10 μm. The image acquisition time was 167 s. (b) SRS spectra of enzyme activities obtained from A549 cells (left) and H226 cells (right). Spectra were obtained from the ROIs shown in Figure S23.

edited 9CN-JCP probes for the detection of enzyme activities in live cells. For this purpose, we selected two human lung carcinoma cell lines A549 and H226, which we found to have different patterns of enzyme activities by using our previously reported HMRG-based fluorescence probes for GGT,[25] LAP,[26] and DPP-4[27] and our HMRef-based fluorescence probe for β-Gal,[28] and by measuring the gene expression levels with quantitative real-time PCR. These results showed that the activities and expression levels of GGT and β-Gal are higher in A549 cells, while those of LAP and DPP-4 are higher in H226 cells (Figures S11 and S12).

We first applied our 9CN-JCP probes individually to live A549 cells and H226 cells to examine whether the probes could visualize the enzyme activities in cells under our SRS microscope. After 30 min incubation with 10 μM gGlu-9CN-JCP, Leu-9C^{15}N-JCP, or EP-9^{13}CN-JCP or with 20 μM βGal-9^{13}C^{15}N-JCP, specific SRS signal activations were observed (Figures S13−S16). Moreover, by taking advantage of the faint red fluorescence emission from the 9CN-JCP scaffolds (Φ_{fl} = 0.055 in PBS(−)), we confirmed that the fluorescence signals of the activated 9CN-JCP probes colocalized well with the SRS signals by dual-mode imaging of SRS and fluorescence (Figures S13−S16). Further, the subcellular localization of these SRS/fluorescence signals is colocalized well with that of

LysoTracker Green, demonstrating that the cleaved dyes (9CN-JCPs) tend to accumulate mainly in lysosomes (Figure S17). We also confirmed that the activation of each probe was inhibited by coincubation with an inhibitor of the corresponding enzyme (Figures S18−S21). The obtained SRS signal intensities were well correlated with the fluorescence intensities, suggesting that evaluation of these enzyme activities with our newly developed Raman probes is reliable (Figure S22).

Finally, we applied our four 9CN-JCP probes simultaneously to A549 cells or H226 cells to examine whether the probes can visualize the different patterns of the four enzyme activities in A549 cells and H226 cells. As shown in Figure 3a,b, the four different enzyme activities were clearly detected as SRS images at distinct Raman frequencies, and the SRS intensities were consistent with those seen when the probes were applied individually. Further, we observed a relatively high background signal in the spectra in cellulo, which is likely to be derived from two-photon absorption (TPA)[29] in EPR condition and cross-phase modulation (XPM),[5,29] which tend to become significant in the presence of cells. However, this background would not affect the accuracy of detection, because the sharp signals of the probes are superimposed on the background, which can easily be subtracted if required. Because these 9CN-

JCP probes are indistinguishable by fluorescence microscopy, this simultaneous detection of the four enzyme activities is a consequence of the sharp Raman signatures (fwhm of the nitrile peak of our 9CN-JCPs is about 15 cm^{-1}), which are highly advantageous for multiplexed imaging. It is particularly noteworthy that the enzyme activities could be detected by using probe concentrations as low as 10−20 μM, owing to the very strong signal activation by shifting molecular absorption from electronic nonresonance conditions to EPR-SRS conditions, and thus the sensitivity is quite high as Raman imaging. Moreover, the spatial resolution of SRS microscopy has been reported to be around 300−400 nm,[10] which is comparable to that of typical confocal fluorescence microscopy. Further, the acquisition time for obtaining SRS images at five different wavenumbers (four wavenumbers for enzyme activities and one wavenumber for background subtraction) was only 2−3 min with our SRS imaging system, which is suitable for live imaging of biomolecules. As we employed 1000-fold signal averaging in these experiments, it would be possible to shorten the acquisition time by averaging fewer signals.

CONCLUSION

In summary, we have established a first-in-class general strategy to prepare activatable Raman probes that show significant enhancement of Raman signals due to a red shift of the molecular absorption upon reaction with the target enzymes. We synthesized several candidate 9CN-pyronines, and evaluation of their optical properties and stability under physiological conditions identified 9CN-JCP as a promising scaffold for activatable Raman probes. We then developed four kinds of activatable Raman imaging probes, gGlu-9CN-JCP, Leu-9C^{15}N-JCP, EP-9^{13}CN-JCP, and βGal-9^{13}C^{15}N-JCP, which exhibit separate sharp Raman peaks and are targeted to different enzyme activities. By applying these four activatable probes to live cells, we succeeded in simultaneous imaging of the four enzyme activities in live cells. To our knowledge, this is the first demonstration of activatable Raman probes that can report enzyme activities under physiological conditions. To expand the color palette, we are planning to develop other scaffolds with peak numbers 15 cm^{-1} apart from that of 9CN-JCP, which might enable us to add four more colors, considering that the fwhm of the nitrile peak of 9CN-JCPs is about 15 cm^{-1} and that isotope-editing shifts the peak wavenumber by about 30 cm^{-1}. To further expand the color variation, we are also planning to replace the nitrile group with an alkyne moiety, which has a peak wavenumber well away from those of nitriles (at around 2180 cm^{-1}). We also anticipate that the wavenumber of the alkyne group can be varied more markedly by the chemical modification, thus opening up the prospect of supermultiplex imaging. Because various enzyme activities are up- or down-regulated in many diseases,[30,31] methodology for simultaneous detection of plural enzyme activities is expected to increase our understanding of the heterogeneity and complexity of diseases. These probes are also promising candidates as tools for precise and early diagnosis of disease. Furthermore, our design strategy for activatable Raman probes should be generally applicable for developing activatable Raman probes targeted to other specific biomolecules or biological processes by leveraging available molecular design strategies for activatable "fluorescent" probes. Therefore, we believe multiplex imaging with these function-

alized Raman probes will be a powerful tool for studying complex biological and pathological phenomena.

ASSOCIATED CONTENT

SI Supporting Information

The Supporting Information is available free of charge at https://pubs.acs.org/doi/10.1021/jacs.0c09200.

Materials and methods, synthetic procedures and characterization of compounds, detailed experimental procedures, spectroscopic data, fluorescence, and SRS imaging results (PDF)

AUTHOR INFORMATION

Corresponding Authors

Yasuyuki Ozeki − *Department of Electrical Engineering and Information Systems, Graduate School of Engineering, The University of Tokyo, Tokyo 113-0033, Japan*; Email: ozeki@ee.t.u-tokyo.ac.jp

Mako Kamiya − *Graduate School of Medicine, The University of Tokyo, Tokyo 113-0033, Japan*; orcid.org/0000-0002-5592-1849; Email: mkamiya@m.u-tokyo.ac.jp

Authors

Hiroyoshi Fujioka − *Graduate School of Pharmaceutical Sciences, The University of Tokyo, Tokyo 113-0033, Japan*; orcid.org/0000-0003-1904-0566

Jingwen Shou − *Department of Electrical Engineering and Information Systems, Graduate School of Engineering, The University of Tokyo, Tokyo 113-0033, Japan*

Ryosuke Kojima − *Graduate School of Medicine, The University of Tokyo, Tokyo 113-0033, Japan; PRESTO, Japan Science and Technology Agency, Saitama 332-0012, Japan*; orcid.org/0000-0002-3792-9222

Yasuteru Urano − *Graduate School of Pharmaceutical Sciences and Graduate School of Medicine, The University of Tokyo, Tokyo 113-0033, Japan*; orcid.org/0000-0002-1220-6327

Complete contact information is available at:
https://pubs.acs.org/10.1021/jacs.0c09200

Author Contributions

All authors contributed to the writing of the manuscript and have given approval to the final version of the manuscript.

Notes

The authors declare the following competing financial interest(s): H.F., J.S., Y.U., Y.O., and M.K are inventors of a patent application covering activatable Raman probes.

■ REFERENCES

(1) Puppels, G. J.; de Mul, F. F.; Otto, C.; Greve, J.; Robert-Nicoud, M.; Arndt-Jovin, D. J.; Jovin, T. M. Studying single living cells and chromosomes by confocal Raman microspectroscopy. *Nature* **1990**, *347* (6290), 301–3.

(2) Sijtsema, N. M.; Wouters, S. D.; De Grauw, C. J.; Otto, C.; Greve, J. Confocal Direct Imaging Raman Microscope: Design and Applications in Biology. *Appl. Spectrosc.* **1998**, *52* (3), 348–355.

(3) Krafft, C. Bioanalytical applications of Raman spectroscopy. *Anal. Bioanal. Chem.* **2004**, *378* (1), 60–2.

(4) Freudiger, C. W.; Min, W.; Saar, B. G.; Lu, S.; Holtom, G. R.; He, C.; Tsai, J. C.; Kang, J. X.; Xie, X. S. Label-free biomedical imaging with high sensitivity by stimulated Raman scattering microscopy. *Science* **2008**, *322* (5909), 1857–61.

(5) Ozeki, Y.; Dake, F.; Kajiyama, S.; Fukui, K.; Itoh, K. Analysis and experimental assessment of the sensitivity of stimulated Raman scattering microscopy. *Opt. Express* **2009**, *17* (5), 3651–8.

(6) Nandakumar, P.; Kovalev, A.; Volkmer, A. Vibrational imaging based on stimulated Raman scattering microscopy. *New J. Phys.* **2009**, *11* (3).

(7) Yamakoshi, H.; Dodo, K.; Okada, M.; Ando, J.; Palonpon, A.; Fujita, K.; Kawata, S.; Sodeoka, M. Imaging of EdU, an alkyne-tagged cell proliferation probe, by Raman microscopy. *J. Am. Chem. Soc.* **2011**, *133* (16), 6102–5.

(8) Chen, Z.; Paley, D. W.; Wei, L.; Weisman, A. L.; Friesner, R. A.; Nuckolls, C.; Min, W. Multicolor live-cell chemical imaging by isotopically edited alkyne vibrational palette. *J. Am. Chem. Soc.* **2014**, *136* (22), 8027–33.

(9) Shi, L.; Zheng, C.; Shen, Y.; Chen, Z.; Silveira, E. S.; Zhang, L.; Wei, M.; Liu, C.; de Sena-Tomas, C.; Targoff, K.; Min, W. Optical imaging of metabolic dynamics in animals. *Nat. Commun.* **2018**, *9* (1), 2995.

(10) Hu, F.; Shi, L.; Min, W. Biological imaging of chemical bonds by stimulated Raman scattering microscopy. *Nat. Methods* **2019**, *16* (9), 830–842.

(11) Wei, L.; Chen, Z.; Shi, L.; Long, R.; Anzalone, A. V.; Zhang, L.; Hu, F.; Yuste, R.; Cornish, V. W.; Min, W. Super-multiplex vibrational imaging. *Nature* **2017**, *544* (7651), 465–470.

(12) Hu, F.; Zeng, C.; Long, R.; Miao, Y.; Wei, L.; Xu, Q.; Min, W. Supermultiplexed optical imaging and barcoding with engineered polyynes. *Nat. Methods* **2018**, *15* (3), 194–200.

(13) Wei, L.; Min, W. Electronic Preresonance Stimulated Raman Scattering Microscopy. *J. Phys. Chem. Lett.* **2018**, *9* (15), 4294–4301.

(14) Yamakoshi, H.; Palonpon, A. F.; Dodo, K.; Ando, J.; Kawata, S.; Fujita, K.; Sodeoka, M. Simultaneous imaging of protonated and deprotonated carbonylcyanide p-trifluoromethoxyphenylhydrazone in live cells by Raman microscopy. *Chem. Commun. (Cambridge, U. K.)* **2014**, *50* (11), 1341–3.

(15) Zeng, C.; Hu, F.; Long, R.; Min, W. A ratiometric Raman probe for live-cell imaging of hydrogen sulfide in mitochondria by stimulated Raman scattering. *Analyst* **2018**, *143* (20), 4844–4848.

(16) Yamaguchi, S.; Matsushita, T.; Izuta, S.; Katada, S.; Ura, M.; Ikeda, T.; Hayashi, G.; Suzuki, Y.; Kobayashi, K.; Tokunaga, K.; Ozeki, Y.; Okamoto, A. Chemically-activatable alkyne-tagged probe for imaging microdomains in lipid bilayer membranes. *Sci. Rep.* **2017**, *7*, 41007.

(17) Chyan, W.; Raines, R. T. Enzyme-Activated Fluorogenic Probes for Live-Cell and in Vivo Imaging. *ACS Chem. Biol.* **2018**, *13* (7), 1810–1823.

(18) Beija, M.; Afonso, C. A.; Martinho, J. M. Synthesis and applications of Rhodamine derivatives as fluorescent probes. *Chem. Soc. Rev.* **2009**, *38* (8), 2410–33.

(19) Ozeki, Y.; Asai, T.; Shou, J.; Yoshimi, H. Multicolor Stimulated Raman Scattering Microscopy With Fast Wavelength-Tunable Yb Fiber Laser. *IEEE J. Sel. Top. Quantum Electron.* **2019**, *25* (1), 1–11.

(20) Shi, J.; Zhang, X.-P.; Neckers, D. C. Xanthenes: Flourone Derivatives II. *Tetrahedron Lett.* **1993**, *34* (38), 6013–6016.

(21) Xiong, H.; Qian, N.; Miao, Y.; Zhao, Z.; Min, W. Stimulated Raman Excited Fluorescence Spectroscopy of Visible Dyes. *J. Phys. Chem. Lett.* **2019**, *10* (13), 3563–3570.

(22) Morozumi, A.; Kamiya, M.; Uno, S. N.; Umezawa, K.; Kojima, R.; Yoshihara, T.; Tobita, S.; Urano, Y. Spontaneously Blinking Fluorophores Based on Nucleophilic Addition/Dissociation of Intracellular Glutathione for Live-Cell Super-resolution Imaging. *J. Am. Chem. Soc.* **2020**, *142* (21), 9625–9633.

(23) Meister, A.; Anderson, M. E. Glutathione. *Annu. Rev. Biochem.* **1983**, *52*, 711–60.

(24) Yamakoshi, H.; Dodo, K.; Palonpon, A.; Ando, J.; Fujita, K.; Kawata, S.; Sodeoka, M. Alkyne-tag Raman imaging for visualization of mobile small molecules in live cells. *J. Am. Chem. Soc.* **2012**, *134* (51), 20681–9.

(25) Urano, Y.; Sakabe, M.; Kosaka, N.; Ogawa, M.; Mitsunaga, M.; Asanuma, D.; Kamiya, M.; Young, M. R.; Nagano, T.; Choyke, P. L.; Kobayashi, H. Rapid cancer detection by topically spraying a gamma-glutamyltranspeptidase-activated fluorescent probe. *Sci. Transl. Med.* **2011**, *3* (110), 110ra119.

(26) Sakabe, M.; Asanuma, D.; Kamiya, M.; Iwatate, R. J.; Hanaoka, K.; Terai, T.; Nagano, T.; Urano, Y. Rational design of highly sensitive fluorescence probes for protease and glycosidase based on precisely controlled spirocyclization. *J. Am. Chem. Soc.* **2013**, *135* (1), 409–14.

(27) Onoyama, H.; Kamiya, M.; Kuriki, Y.; Komatsu, T.; Abe, H.; Tsuji, Y.; Yagi, K.; Yamagata, Y.; Aikou, S.; Nishida, M.; Mori, K.; Yamashita, H.; Fujishiro, M.; Nomura, S.; Shimizu, N.; Fukayama, M.; Koike, K.; Urano, Y.; Seto, Y. Rapid and sensitive detection of early esophageal squamous cell carcinoma with fluorescence probe targeting dipeptidylpeptidase IV. *Sci. Rep.* **2016**, *6*, 26399.

(28) Asanuma, D.; Sakabe, M.; Kamiya, M.; Yamamoto, K.; Hiratake, J.; Ogawa, M.; Kosaka, N.; Choyke, P. L.; Nagano, T.; Kobayashi, H.; Urano, Y. Sensitive beta-galactosidase-targeting fluorescence probe for visualizing small peritoneal metastatic tumours in vivo. *Nat. Commun.* **2015**, *6*, 6463.

(29) Cheng, J. X.; Xie, X. S. *Coherent Raman Scattering Microscopy*; Taylor & Francis, 2012.

(30) Artal-Sanz, M.; Tavernarakis, N. Proteolytic mechanisms in necrotic cell death and neurodegeneration. *FEBS Lett.* **2005**, *579* (15), 3287–96.

(31) Lopez-Otin, C.; Matrisian, L. M. Emerging roles of proteases in tumour suppression. *Nat. Rev. Cancer* **2007**, *7* (10), 800–8.